

Design of Novel Photoactive Modified Titanium Silicalites and Their Application for Venlafaxine Degradation under Simulated Solar Irradiation

Guillermo Cruz-Quesada, Maria J. Sampaio, Maialen Espinal-Viguri, María Victoria López-Ramón, Julián J. Garrido,* Cláudia G. Silva, and Joaquim L. Faria*

Titanium silicalites (TS) are well-known materials for their use in industrial oxidation reactions, and although they are used as photocatalysts, their activity is limited. Therefore, numerous synthetic strategies are investigated to improve their photocatalytic activity. Herein, three series of modified titanium silicalites are synthesized using three different organotriethoxysilanes at different molar percentages with the aim of modifying the structure of the zeolite, both at a porous and chemical level, to obtain materials with high photocatalytic activity. The study of their morphological, textural, chemical, and UV-vis light absorption properties through various characterization techniques has allowed the selection of the best candidates to test their photoactivity in the degradation of venlafaxine, an antidepressant drug that persists as a contaminant in wastewater and has serious neurotoxic effects. Materials synthesized using a 5% molar percentage of RTEOS and 10% of PhTEOS (Ph = phenyl) are able to degrade venlafaxine, whereas the reference material does not show any photocatalytic activity. These results lead the way to use this synthetic strategy to develop titanium silicates and optimize their photocatalytic activity in degradation reactions of different pollutants.

technologies, photocatalysis stands out for its recent advances in contaminant removal^[1–4] or hydrogen production.^[5–7] With these applications in mind, semiconductor materials of diverse nature and composition have been designed, such as metal-organic frameworks,^[3,7] metal-carbon composites,^[2,8] g-C₃N₄ composites,^[5,9] or TiO₂-based materials,^[4,6] among others. The objectives to be achieved in the preparation of photocatalysts are the improvement of the energy conversion efficiency and photochemical stability, the expansion of the excitation spectral range toward the visible, and the development of simple and low-cost synthesis methodologies that are scalable at the industrial level.^[10–15] Due to the difficulty of achieving all these objectives, just a few commercial catalysts are currently available. In this regard, metal oxides, especially titanium dioxide (TiO₂), are among the most promising optical semiconductor materials for applications


1. Introduction

In recent decades, a deep interest has arisen in developing more efficient technologies to alleviate the consequences of human activity on the environment. Among the most promising

in photocatalysis, mainly due to their high stability, high oxidizing power, and low manufacturing cost. However, the biggest drawback of TiO₂ is that even the most commercialized photocatalyst (Degussa P25) only absorbs in the UV range, limiting solar applications.^[16]

G. Cruz-Quesada, M. Espinal-Viguri, J. J. Garrido
Department of Science
Institute for Advanced Materials and Mathematics (INAMAT2), Public
University of Navarre (UPNA)
Campus Arrosadía, 31006 Pamplona, Spain
E-mail: j.garrido@unavarra.es

M. J. Sampaio, C. G. Silva, J. L. Faria
LSRE-LCM - Laboratory of Separation and Reaction Engineering –
Laboratory of Catalysis and Materials
Faculty of Engineering
University of Porto
Rua Dr. Roberto Frias, 4200-465 Porto, Portugal
E-mail: jlfaria@fe.up.pt

 The ORCID identification number(s) for the author(s) of this article can be found under <https://doi.org/10.1002/solr.202300593>.

M. J. Sampaio, C. G. Silva, J. L. Faria
ALiCE - Associate Laboratory in Chemical Engineering
Faculty of Engineering
University of Porto
Rua Dr. Roberto Frias, 4200-465 Porto, Portugal

© 2023 The Authors. Solar RRL published by Wiley-VCH GmbH. This is an open access article under the terms of the Creative Commons Attribution-NonCommercial License, which permits use, distribution and reproduction in any medium, provided the original work is properly cited and is not used for commercial purposes.

M. V. López-Ramón
Department of Inorganic and Organic Chemistry
Faculty of Experimental Sciences
University of Jaen
23071 Jaen, Spain

DOI: 10.1002/solr.202300593

Titanium silicalites (TSs), Ti-containing zeolites first synthesized by Tamarrasso in 1983,^[17] emerged as promising materials for photocatalysis. These materials are mainly known to be used as molecular sieves and as catalysts in industrial reactions of great interest such as olefin epoxidation,^[18,19] oxidative desulfurization,^[20] or hydroxylation of alkanes and aromatic compounds^[21]. TSs are photoactive materials under excitation with UV–vis radiation; therefore, besides being useful in the aforementioned oxidation reactions, they have also been used as photocatalysts in the production of H₂,^[22–24] in the photodegradation of pollutants in an aqueous media,^[25–27] and in the photoepoxidation of propylene,^[28] among others.

The most representative form of titanium in the TSs framework is Ti⁴⁺, which exhibits a tetrahedral coordination geometry (TiO₄) and is locally distributed throughout the modernite framework inverted silicalite structure (MFI). When TiO₄ species are excited with UV–vis light, a charge transfer takes place from one of the coordinating oxygen atoms (O^{2−}) to the Ti⁴⁺ cation, yielding in the process an electron–hole pair as the excited state (Ti³⁺–O[−]), which is responsible for the material's photoactivity.^[29,30] However, the size difference between Si and Ti atoms makes it difficult to synthesize a TS with a titanium content higher than 2.5 wt% without modifying the crystalline structure.^[31] For this reason, defective Ti⁴⁺ species, such as partially coordinated (TiO₃OH), pentacoordinated (TiO₅), or octahedrally coordinated (TiO₆) species, can be found in TSs.^[32–34] Additionally, depending on the synthesis conditions, anatase can be formed (TiO₂, mainly TiO₆) because the titanium precursors (tetrabutoxides, isopropoxides...) rapidly hydrolyze (5–10 min) and condense with each other rather than with the silicon precursors, which present a slower hydrolyzation (1.5 h).^[35] The presence of anatase in the final material is not desirable because TiO₄ species exhibit much higher photocatalytic activity than TiO₆.^[36] Therefore, the need to obtain TS with a high TiO₄ content is still a challenge and has led to the development of strategies to slow down the hydrolysis of Ti precursors using complexing agents such as H₂O₂, acetylacetonate, or isopropanol.^[37] In this context, Ma et al. reported that polyvinylpyrrolidone (PVP) acts as a structure-directing agent (SDA) in the synthesis of TSs, competing with commonly used surfactants, such as TPAOH, and regulating the nanostructuration of the silica skeleton.^[38] In addition, PVP decreases the condensation rate once the titanium precursor is hydrolyzed, favoring its crosslinking with the hydrolyzed silica precursor.

In the present work, a new synthetic approach is proposed, in which in addition to TPAOH, PVP, tetraethoxysilane (TEOS), and a titanium precursor, different molar proportions of an organotriethoxysilane have been used (RTEOS, R = methyl, M; propyl, P; and phenyl, Ph) yielding three series of modified titanium silicalites (TSR%). This strategy aims to achieve a change in the internal morphology and structure of the TSR% silica skeleton, as well as in their porous texture, surface chemistry, and proportion of titanium species (TiO₄/TiO₆) to obtain materials with greater photocatalytic activity. In this regard, RTEOS acts as an additional SDA for the construction of the MFI zeolite skeleton, and its organic moiety blocks one of the positions susceptible to hydrolyzing and condensing, thus conditioning the internal structure of the material and yielding a variety of porous textures depending on the organosilane and its molar percentage

used in the synthesis. In addition, this organic moiety has less electron withdrawal than the ethoxide groups, and since polycondensation follows a type 2 nucleophilic substitution mechanism (due to the basicity of the medium), its use will slow down the reaction, which will also affect the final morphology of the materials.^[39] After an exhaustive characterization in which the properties of the prepared materials were elucidated and discussed (UV–vis absorption, photoluminescence (PL) emission, nanostructuration, N₂ and CO₂ adsorption capacity, morphology), it was determined that the most promising materials for photocatalysis were those synthesized with 5% RTEOS (TSR5, R = methyl, propyl and phenyl) and the material synthesized with 10% PhTEOS (TSPH10). Once those materials were selected, their activity in the degradation of venlafaxine, a contaminant included in the European Union's Watch List of Substances,^[40] was tested. The new TSR5 materials, unlike the reference material synthesized under the same conditions without RTEOS, were able to almost degrade venlafaxine completely in less than two hours, confirming that this synthetic approach can lead to an improvement and easy modulation of the photocatalytic properties of titanium silicalites due to the chemical, structural, and textural changes derived from the introduction of RTEOS in the synthesis.

2. Results and Discussion

2.1. Titanium Silicalites (TS) Preparation

The synthesis method to prepare the titanium silicalites (TS) is based on the one described by W. Ma et al.^[38] **Figure 1** displays the scheme of the synthesis and the code list for the synthesized materials and the specifications of the reagents used. The detailed procedure of the modified TSs preparation can be found in Section S1, Supporting Information.

2.2. Characterization Analysis of the Synthesized Materials

2.2.1. X-ray Diffraction (XRD)

Figure 2 depicts the diffraction patterns of the materials obtained in the range 5° < 2θ < 35°.

The diffraction patterns show that the TSR5, TSR10, TSPH20, and TSPH30 materials present diffraction maxima at 7.8°, 8.9°, 23.1°, 24°, and 24.5°, consistent with the standard diffraction patterns of TS-1 (ICDD, JCPDS, file code 70-4276). In the literature, these maxima are associated with (101), (200), (501), (151), and (313) orthorhombic MFI lattice planes, respectively, where the Ti⁴⁺ cations are substituting silicon atoms in the framework.^[26,41] However, the diffraction pattern of the reference material shows that the diffraction maximum at 24.5° is split, which indicates that this material is monoclinic, as happens with highly pure silicalites ([Si₉₆O₁₉₂]), suggesting that only part of the Ti⁴⁺ cations are successfully embedded in the silica framework.^[42] On the contrary, this split is not observed in the diffraction patterns of the TSR materials and additionally, as the molar percentage of organotriethoxysilane (RTEOS) increases from 5 to 10%, this maximum gets sharper, denoting that the precursor aids the incorporation of Ti⁴⁺.

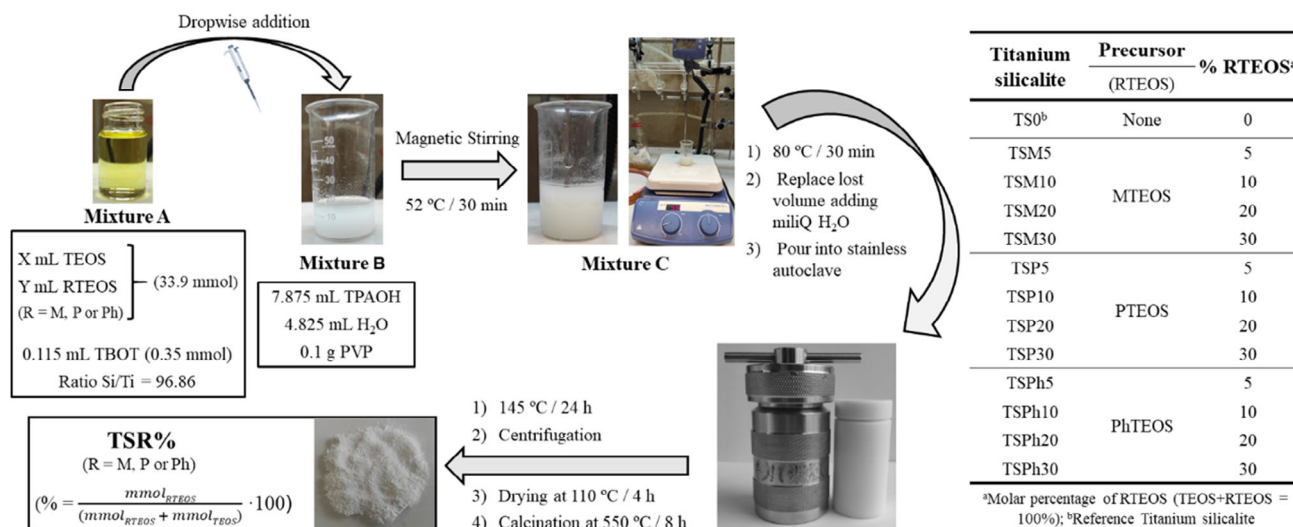


Figure 1. Synthesis procedure and nomenclature of the modified titanium silicalites.

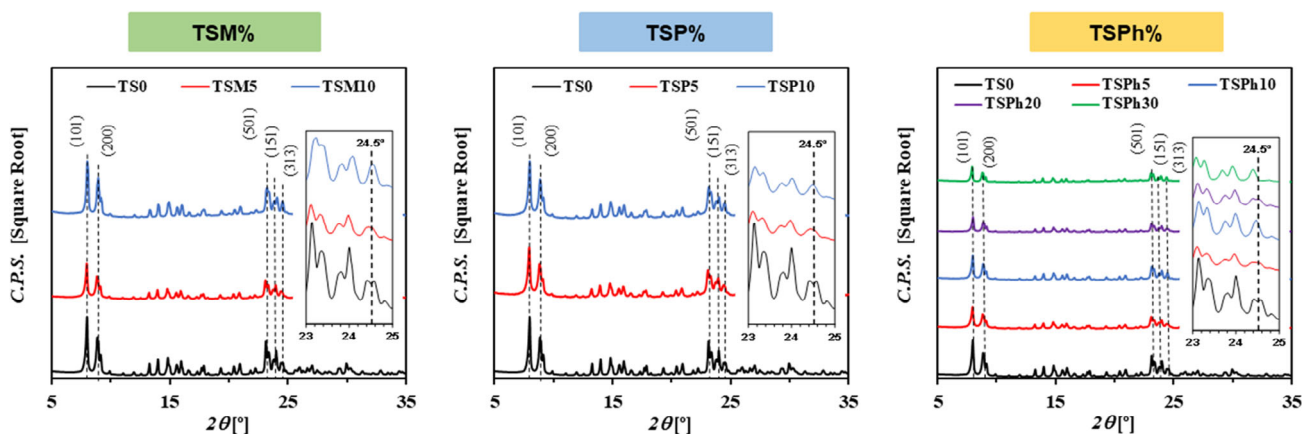


Figure 2. XRD patterns of the reference material (TS0, in black) and the TSR% materials.

The diffraction patterns of TSPPh20 and TSPPh30 show the characteristic maxima of titanium silicalite-1 (TS-1), while those of TSM20, TSM30, TSP20, and TSP30 do not present these maxima, and only a broad maximum at 23° is observed (Figure S1, Supporting Information). This maximum is associated with the siloxane bonds (Si—O—Si) of amorphous silica, indicating that increasing the amount of alkyltriethoxysilane beyond 10% molar percentage restrains the formation of MFI-type structures. It is worth mentioning that the diffraction patterns of all the materials do not present a maximum at $2\theta = 25.4^\circ$; therefore, the presence of extraframework Ti^{4+} in the form of anatase can be ruled out (JCPDS file 73-1764).

2.2.2. Fourier-Transform Infrared Spectroscopy (FTIR)

Figure 3 displays the Fourier-transform infrared spectroscopy (FTIR) spectra of the TSR materials in the spectral range between

1600 and 400 cm^{-1} , and Figure S2, Supporting Information illustrates the spectral region $4000\text{--}2750\text{ cm}^{-1}$. No relevant bands were observed in the $2750\text{--}1600\text{ cm}^{-1}$ range.

A detailed explanation of the observed bands can be found in Section S3, Supporting Information. It is important to note that the intensity of the band at 800 cm^{-1} is a good indicator of the amorphism grade of the material because it corresponds to amorphous silica.^[43] On this basis, in the FTIR spectra, it is easily observable that by increasing the amount of organotriethoxysilane, more amorphous materials are obtained. By comparison with the X-ray diffraction (XRD) patterns, it can be stated that TSR20 and TSR30 derived from MTEOS and PTEOS are completely amorphous, whereas those derived from PhTEOS still retain a certain grade of crystallinity. Regarding the FTIR spectra of TSPPh20, the simultaneous presence of MFI structure bands (1230 and 550 cm^{-1}) and the characteristic band of amorphous silica at 800 cm^{-1} suggest that the material is semi-crystalline, although for TSPPh30 MFI structure, bands are not

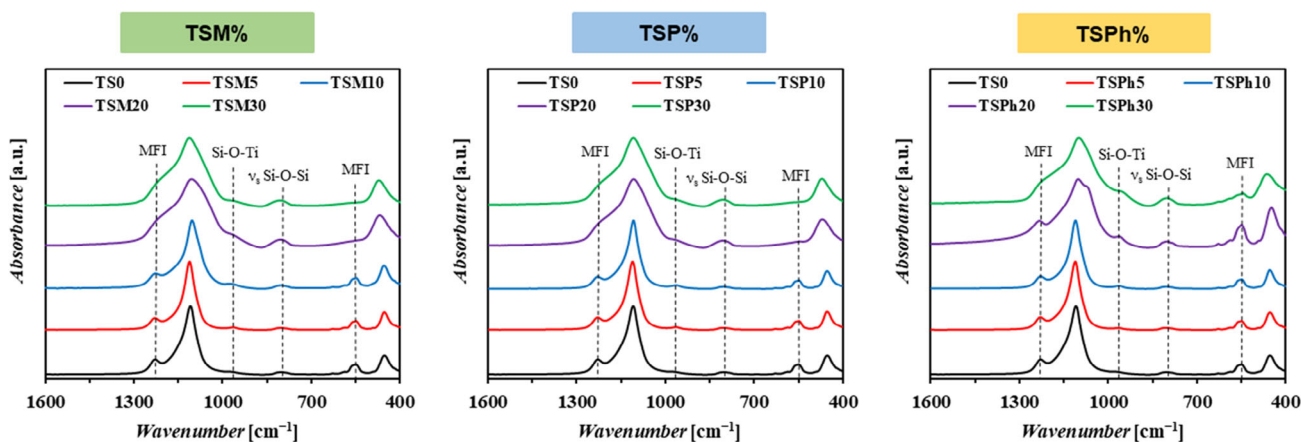


Figure 3. FTIR spectra of TSM%, TSP%, and TSPh% in the 1600–400 cm^{-1} frequency region.

observable, indicating that this material is substantially more amorphous, although based on its XRD pattern (depicted in Figure 2) it retains a certain grade of crystallinity.

2.2.3. Diffuse Reflectance UV–vis, Photoluminescence Emission, and UV–Raman Spectroscopy

Diffuse reflectance (DR) UV–vis spectra of the TSR% materials in the range of 210–410 nm are depicted in Figure 4, and in Section S4, Supporting Information, a theoretical explanation

of the characteristic spectra of the MFI-structured titanium silicates is described.

The spectra of the TSR materials synthesized in this work exhibit the bands attributed to the tetracoordinated titanium embedded in the framework and the extranet hexacoordinated titanium. The band due to the anatase is not observed, thus discarding its presence in the materials, which agrees with the XRD patterns. The absorption intensity at ≈ 213 nm (tetracoordinated titanium band) and at ≈ 265 nm (hexacoordinated titanium band) increases as the amount of RTEOS rises (except for the band at ≈ 213 nm of the TSR5 materials), consistent with the nonsplit

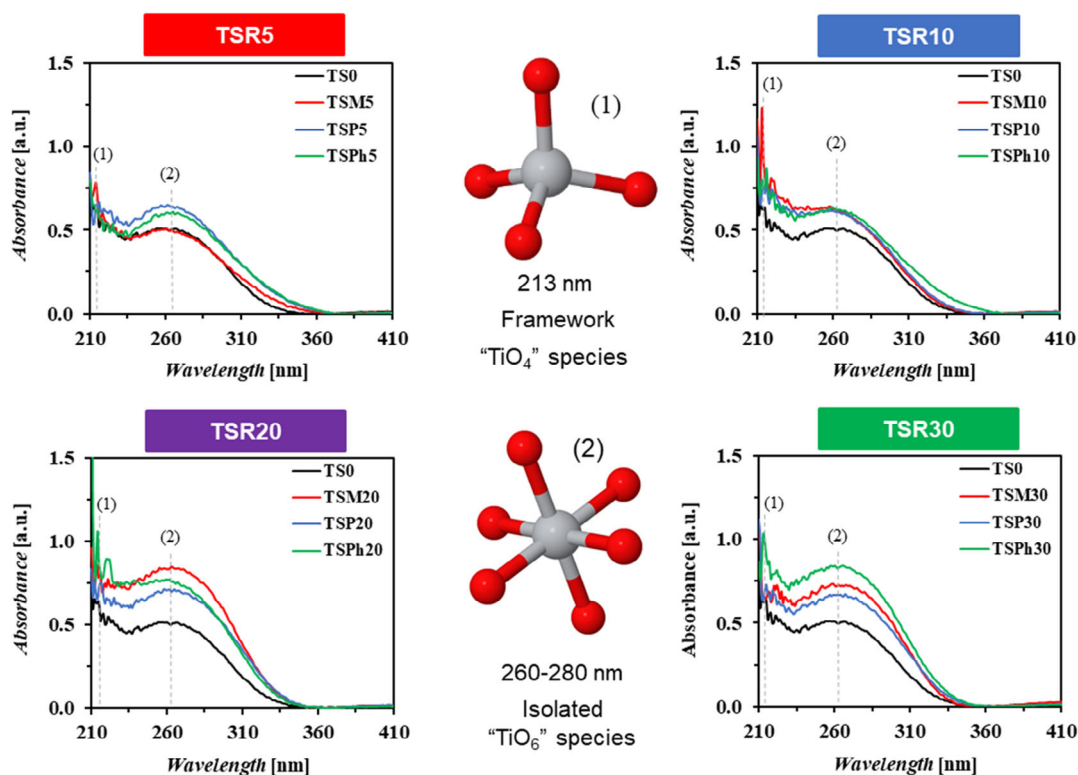


Figure 4. DR UV–vis spectra of reference material and TSR5, TSR10, TSR20, and TSR30.

narrower maximum at $2\theta = 24.5^\circ$ in the XRD (Figure 2). Furthermore, the decay of the ≈ 265 nm absorption band is enlarged from 350 to 370 nm in the TSR5 and TSPH10 materials, which is translated in a larger range of absorption and will be of great relevance in their photocatalytic activity.

Information on the electronic structure of these materials was obtained by applying the Tauc plot analysis to the UV-vis spectra data (Figure S3, Section S4, Supporting Information).^[44] The indirect-bandgap values obtained for the TSR materials are lower than 4 eV, implying that they might exhibit photocatalytic activity; moreover, all the materials yielded lower bandgap values than TS0. Remarkably, TSPH5 and TSPH10 are the materials with the lowest bandgap values when compared to their analogues with the same molar percentage of RTEOS.

The PL emission spectra of the TSR5 and TSR10 materials are illustrated in Figure 5 and S4, Supporting Information depicts those of TR20 and TR30.

The PL emission spectra of the materials were obtained at 260 nm, which is the maximum UV-vis absorption of the hexacoordinated Ti species, and 370 nm, which is the limit of UV absorption of TSR5 and TSPH10 (Figure 4). When the materials are excited at 260 nm, a set of bands in the range of 400–500 nm is observed, attributed to the radiative decay process from the charge transfer between O^{-2} and Ti^{+4} .^[45] At this wavelength, the emission intensity decreases as the molar percentage of

RTEOS increases, implying that these modified titanium silicalites present a lower recombination rate of the electron-hole pair than the ref. [28]. However, when they are excited at 370 nm, TSM5 presents an intensity similar to that of the reference, whereas TSP5, TSPH5, and TSPH10 intensity is lower than TS0, and TSM10 and TSP10 intensity is higher. These observations, together with the information elucidated by the UV-vis absorption, suggest that TSP5, TSPH5, and TSPH10 might exhibit the highest photocatalytic activity among the synthesized titanium silicalites.

UV-Raman spectra at 325 nm of TSR5 and TSR10 samples were acquired to further delve into the relative proportion of Ti species in the samples (Figure S5, Supporting Information). The UV-Raman spectrum of the reference (TS0) shows some of the characteristic bands of the MFI structures at 290, 380, and 800 cm^{-1} . Additionally, a low-intensity band associated with the asymmetric stretching vibration of TiO_4 species is detected at ≈ 960 cm^{-1} , while the symmetric stretching vibration usually reported at 1125 cm^{-1} is not observable.^[33] Remarkably, the intensity of the 380 cm^{-1} band of TSR5 and TSR10 is considerably lower, which points to the gradual loss of crystallinity produced by the use of the organosilanes. TSM10 spectrum is the only one that clearly depicts the 960 cm^{-1} band, thus confirming the presence of a TiO_4 framework in the material. However, an emerging band at ≈ 700 cm^{-1} in the TSR5 and TSPH10 spectra is noticeable, which is more

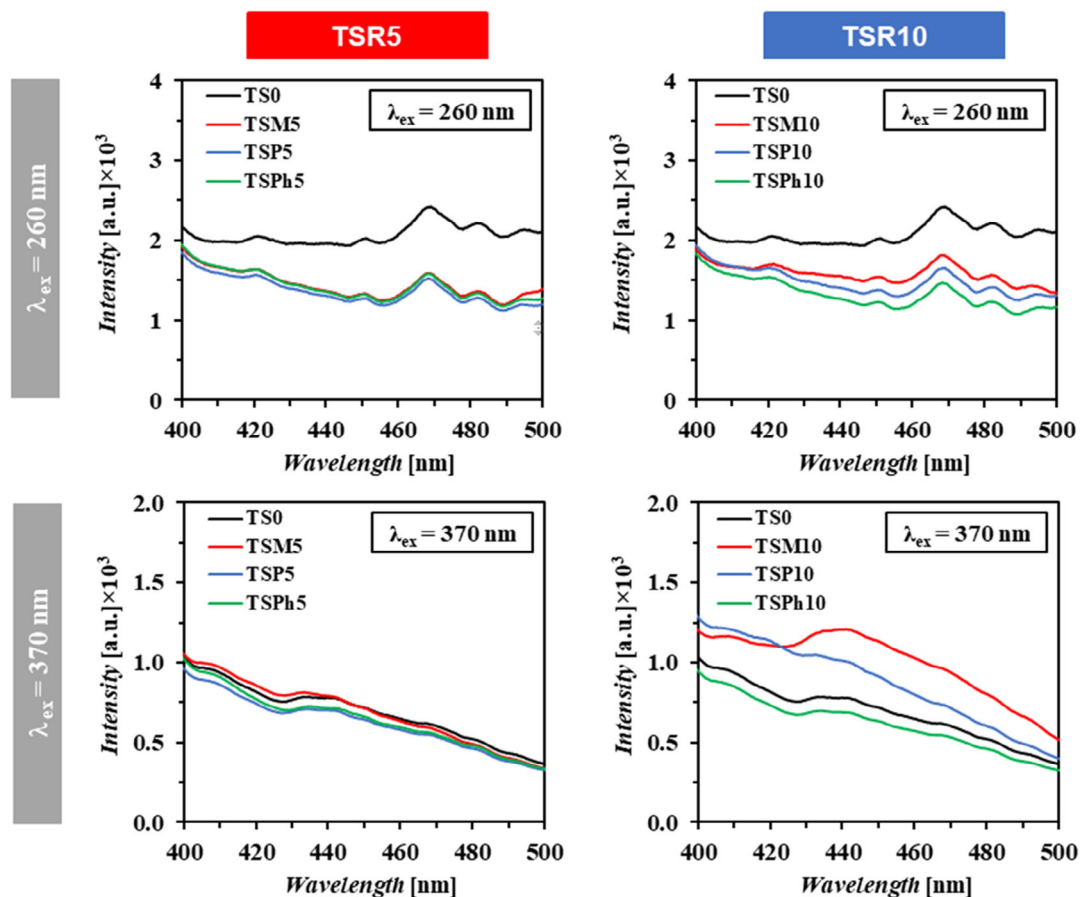


Figure 5. Photoluminescent emission spectra of TSR5 and TSR10 materials registered at 260 and 370 nm excitation wavelength.

intense in the TSPH5 and TSPH10 materials. In the literature, the presence of a band at 695 cm^{-1} has been associated with the UV–vis absorption band at 270 nm of titanium silicalites and therefore, with the Ti–O stretching vibration of TiO_6 octahedron species (i.e., amorphous Ti).^[33] Hence, the use of organosilanes in titanium silicalite synthesis, especially phenyltriethoxysilane, is detrimental to the formation of TiO_4 framework species and helps the formation of superficial amorphous TiO_6 species. Thereby, the enlarger UV–vis absorption range and the lower PL emission intensity of TSR5 and TSPH10 materials are a consequence of the higher proportion of such species.

2.2.4. N_2 and CO_2 Adsorption

Figure 6 displays the N_2 adsorption isotherms obtained for TSR5 and TSR10 materials (registered at -196°C). N_2 isotherms

of TSR20 and TSR30 and CO_2 isotherms of TSR5 and TSR10 materials are displayed in Figure S6 and S7, Supporting Information, respectively. The textural parameters obtained from the isotherms of both adsorbates are shown in Table 1.

The characteristic N_2 isotherms of MFI zeolites are explained in Section S5. In this work, all the materials which are considered zeolites, including the reference, show a type VI N_2 isotherm, a type H3 hysteresis loop at high partial pressures, and a high adsorption at $p/p_0 < 0.03$, representing more than half of the N_2 adsorption capacity (Table 1), in agreement with other reported MFI zeolites. The reference material shows a type H4 hysteresis loop at $0.1 < p/p_0 < 0.35$ due to adsorbate–adsorbate interactions inside the pores, leading to a framework structural change produced by the deformation of the nonrigid pore walls.^[46] Remarkably, the addition of a 5% molar percentage of RTEOS in the synthesis results in materials with a similar

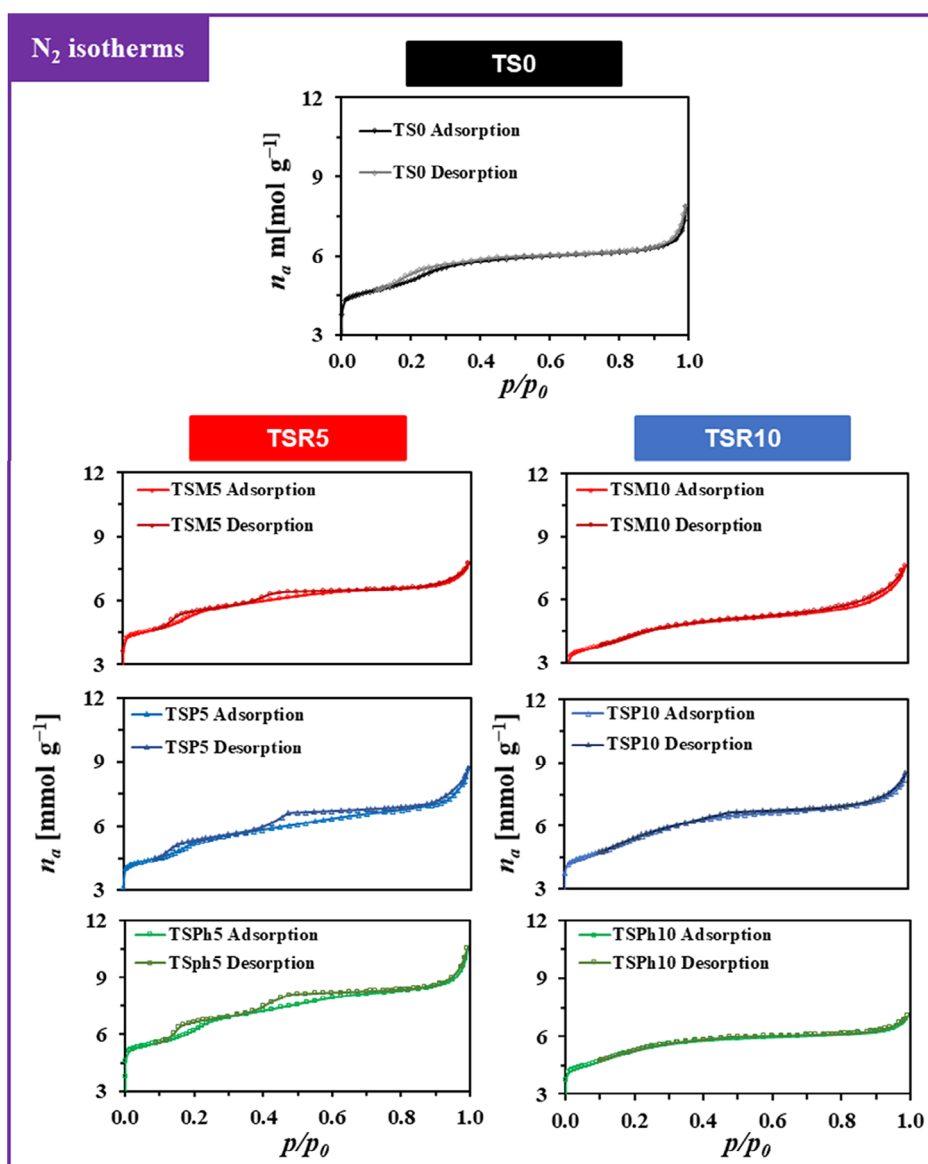


Figure 6. N_2 adsorption isotherms of the reference, TSR5, and TSR10 materials.

Table 1. Textural parameters of the reference, TSR5, and TSR10 materials.

Material	a_{BET}	$V_{\text{micro}}^{\text{a)}}$	$V_{\text{micro}}^{\text{a)}}$	$V_{\text{meso}}^{\text{b)}}$	$V_{\text{macro}}^{\text{c)}}$	$V_{\text{total}}^{\text{d)}}$	$n_{\text{a}}^{\text{e)}}$ ($p/p_0 \leq 0.03$)	$\text{BJH APS}^{\text{f)}$	$E_{\text{c}}^{\text{g)}$	$E_{\text{c}}^{\text{g)}$
	(N_2)	(CO_2)	(N_2)	(N_2)	(N_2)	(N_2)	(N_2)		(N_2)	(CO_2)
	$[\text{m}^2 \text{g}^{-1}]$			$[\text{cm}^3 \text{g}^{-1}]$			[%]	[nm]	$[\text{kJ mol}^{-1}]$	
TS0	420	0.20	0.17	0.06	0.00	0.23	68.28	5.05	26.86	21.60
TSM5	413	0.22	0.16	0.06	0.01	0.24	62.95	4.23	26.38	20.66
TSM10	334	0.15	0.14	0.06	0.03	0.23	53.41	5.72	20.99	22.26
TSP5	399	0.22	0.16	0.08	0.02	0.26	56.76	4.91	27.01	20.33
TSP10	417	0.19	0.17	0.07	0.02	0.26	58.27	4.65	22.61	20.11
TSPH5	499	0.22	0.20	0.09	0.02	0.31	59.49	4.70	26.14	20.55
TSPH10	413	0.23	0.17	0.03	0.02	0.22	67.18	4.28	20.21	21.36

^{a)}Micropore volume obtained from Dubinin–Raduskevich; ^{b)}Mesopore volume obtained from $V_{\text{total}} - V_{\text{micro}(\text{N}_2)} - V_{\text{macro}}$; ^{c)}Macropore volume obtained from isotherm ($V_{p/p_0=0.95} - V_{p/p_0=0.8}$); ^{d)}Total pore volume obtained from isotherm at $p/p_0=0.95$; ^{e)}Amount of N_2 adsorbed at $p/p_0 \leq 0.03$ compared to V_{total} ; ^{f)}APS obtained from desorption branch; ^{g)}Characteristic energy from Dubinin–Raduskevich.

hysteresis loop than the reference at $0.1 < p/p_0 < 0.35$, and a new H4 hysteresis loop located at $0.35 < p/p_0 < 0.8$, consistent with a change in the morphology of the narrow mesopores, from cylindrical to ink-bottle shaped and thus, creating a retention effect of the adsorbate inside the pores and its capillary condensation.^[47] This change in the pore morphology of the TSR5 materials together with their higher pore volume (V_{Total}) and lower amount of N_2 adsorbed at $p/p_0 \leq 0.03$ suggests the possibility of an improvement in the diffusion performance and accessibility of the adsorbates to the active sites during the photocatalysis.^[24] On the contrary, the materials prepared with a 10% molar percentage of RTEOS lack the hysteresis at $0.1 < p/p_0 < 0.35$ observed in TSR5, and their isotherms show a partial loss of the narrow mesoporosity, which is translated in the flattening of the hysteresis at $0.35 < p/p_0 < 0.8$. Finally, materials discarded as zeolites due to their substantial amorphous nature (TSM20, TSM30, TSP20, TSP30, and TSPH30) present type II isotherms, characteristic of macroporous or nonporous solids (Figure S6, Supporting Information). Remarkably, TSPH20, which is a semicrystalline material based on its XRD pattern and FTIR spectrum, presents a type VI isotherm with most of its N_2 adsorption below a partial pressure of 0.03, reinforcing the idea that, although it is partially amorphous, most of its skeleton is nanostructured, granting the material MFI zeolite properties. All the titanium silicalites have similar specific surface areas (a_{BET}) to that of the reference, except TSM10 and TSPH5, consistent with their adsorption capacity. The characteristic energy ($E_{\text{c}(\text{N}_2)}$) decreases with the increase of RTEOS in all the materials, implying a more labile interaction between the surface of the material and the N_2 .

Regarding the CO_2 isotherms (Figure S7, Supporting Information), using 5% of any RTEOS does not significantly affect their micropore volume ($V_{\text{micro}(\text{CO}_2)}$), as these materials and the reference adsorb similar quantities of CO_2 . On the contrary, materials synthesized with 10% RTEOS show relevant changes in the volume of micropores. The micropore volume of TSM10 and TSP10 decreases with respect to the reference, whereas the one of TSPH10 increases. In addition, for all the materials, $V_{\text{micro}(\text{N}_2)} < V_{\text{micro}(\text{CO}_2)}$ (Table 1), confirming that N_2

faces kinetic restraints to enter the narrow micropores. This observation is consistent with their ultramicroporous nature,^[37] although based on the average pore size (APS) determined by the Barret–Joyner–Halenda method (BJH), all the materials retain a certain degree of mesoporosity.

The pore size distributions (PSD) of the materials using both adsorbates have been determined by density functional theory (DFT) methods and are shown in Figure 7.

This figure illustrates that most of the pores have an internal diameter (ϕ) centered at ≈ 0.6 nm for both adsorbates. This is to be expected since zeolites with MFI-type structures, such as titanium silicalites, are formed of ten-membered rings ($(\text{SiO})_{10}$), with internal diameter channels of $\phi = 0.55$ nm,^[48] which means that only small molecules such as N_2 or CO_2 ($\phi = 0.36$ and 0.33 nm, respectively) are able to access the pores. N_2 PSD of all materials are characteristic of ultramicroporous materials with a slight portion of narrow mesopores centered at $\phi = 2\text{--}4$ nm.

2.2.5. FESEM and EDX

To determine the particle size and morphology, micrographs of the materials were acquired using field-emission scanning electron microscopy (FESEM). The micrographs of TSR5 and TSPH10 are displayed in Figure 8.

The micrograph of TS0 exhibits an agglomeration of ellipsoidal particles with smooth surfaces and variable sizes (ranging from 250 to 320 nm). This morphology differs from the characteristic coffin-like hexagonal crystal shape of titanium-silicalites prepared with TPA^+ as the only SDA.^[49] The shape of the particles in this material derives from the presence of PVP in the synthesis media, which not only slows down the TBOT hydrolysis aiding the introduction of titanium in the matrix but also competes with the TPA^+ cation acting as a surfactant. This competition changes the crystal growth due to the PVP hydrogen bonding interactions within the TS skeleton,^[38] yielding flat-cylinder-shaped particles with smaller sizes than titanium silicalites synthesized by similar procedures ($0.5\text{--}3$ μm).^[18,50,51] The micrographs of the TSR materials show how the use of

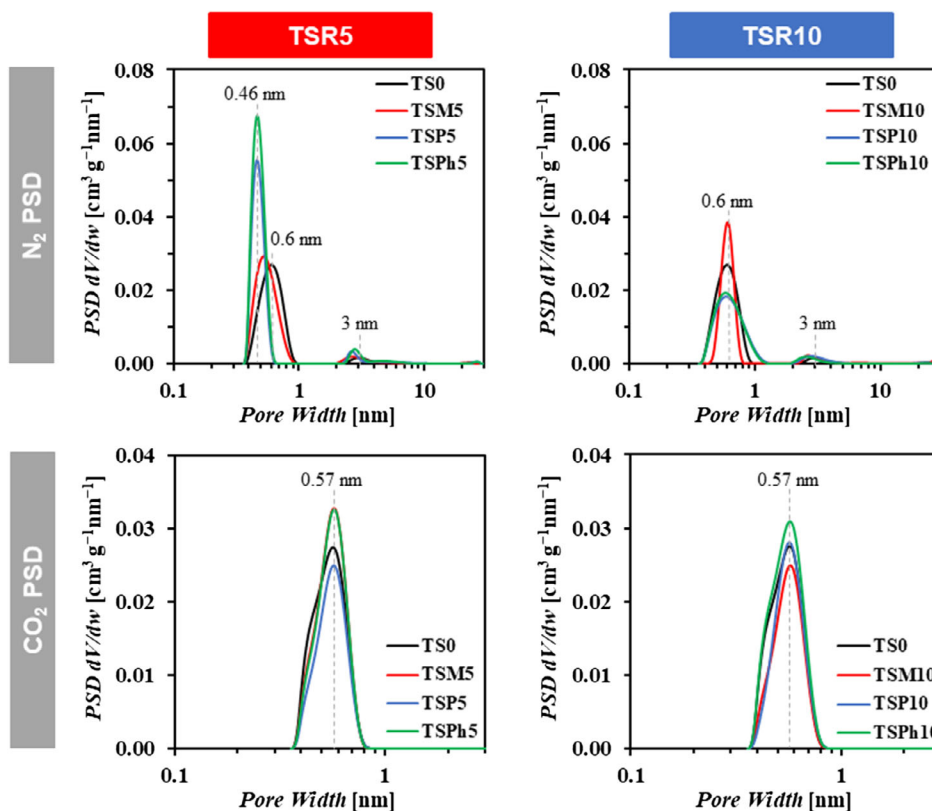


Figure 7. DFT and PSD obtained from the N_2 and CO_2 isotherms data of the reference, TSR5, and TSR10 materials.

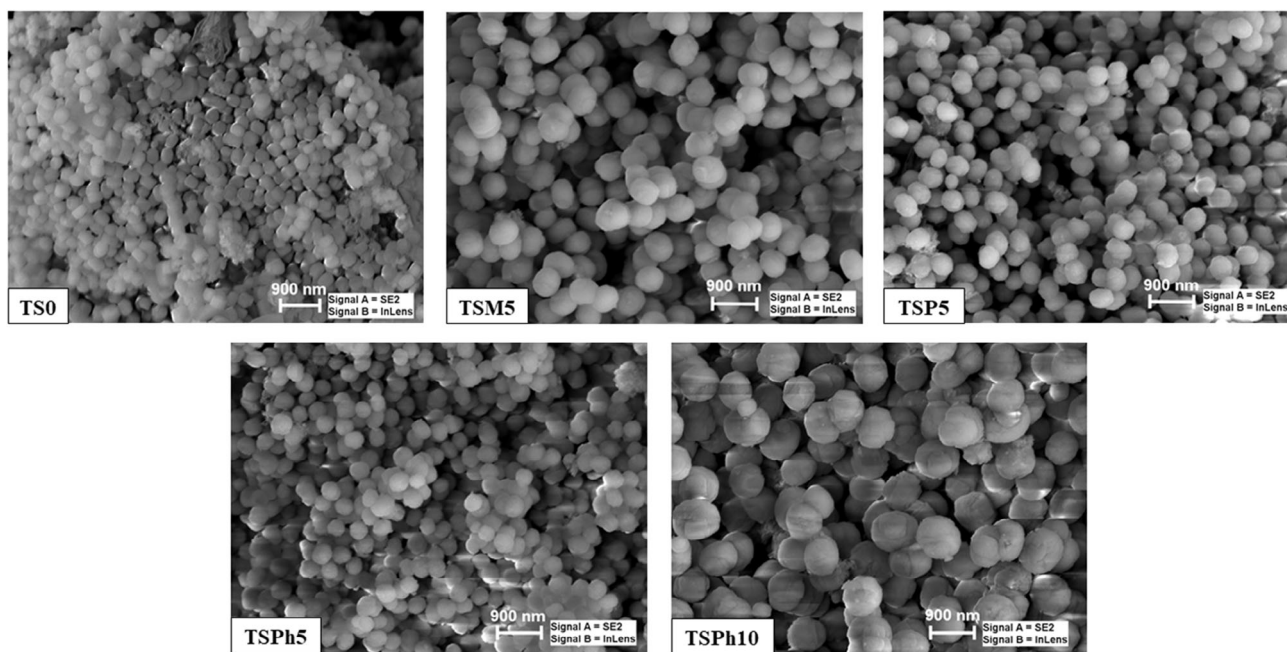


Figure 8. FESEM micrographs of the reference, TSM5, TSP5, TSPh5, and TSPh10 materials.

RTEOS has a big impact on their morphology, as they exhibit bigger, rougher, and more spherical-shaped particles than those of TS0, suggesting that the organic moiety of RTEOS hinders the

surface interaction of the colloids with the SDAs, which might be the reason why more the molar percentage of RTEOS, bigger the particles of the material ($TS0 < TSP5 < TSP10$).

The hindrance exerted by organosilanes may further explain why materials with a high content of RTEOS (TSR20 and TSR30) gradually lose their crystallinity, and therefore, the skeletal density decreases (Table S1 in Section S5, Supporting Information). When the same molar proportion of RTEOS is used, the size of the particles varies depending on the precursor. The material obtained with 5% of PhTEOS exhibits the smallest particle sizes (320–420 nm), whereas the same percentage of MTEOS yields larger particle sizes (550–675 nm), indicating that the methyl group induces a greater steric effect than the phenyl group, hindering the SDAs more effectively and thus, the growth of the particles. The interparticle space observed in the micrographs constitutes the wide mesoporosity and macroporosity, part of which is displayed as a hysteresis loop above 0.9 p/p^0 in the adsorption–desorption isotherms (Figure 6).

To estimate the amount of titanium in the materials, a mapping of the composition was carried out by X-ray energy dispersion. The average values resulting from several mappings are given in Table 2.

Results in Table 2 show that most of the materials contain ≈ 0.9 wt% of titanium, consistent with the previously reported titanium silicalites synthesized under the same conditions.^[38] The presence of carbon in the materials is due to the calcination residues from the organic templates, identified as dust in the micrographs. Surprisingly, TSP5 presents the highest titanium amount out of all the materials. This fact, together with its high-UV–vis absorption and low PL intensity, suggests that TSP5 could be the best candidate as a photocatalyst. However, TSP5 displays various properties which must be in consideration for the catalytic activity: it presents the smallest particle sizes, the biggest surface area, and the highest pore capacity. Furthermore, its UV–Raman spectrum shows a more intense signal of TiO₆ species than TSP5.

2.3. Photocatalytic Degradation of Venlafaxine in the Presence of TS

The photoactivity of TSR materials was tested in the degradation of 5 ppm aqueous solutions of venlafaxine under simulated solar irradiation for 1 h. TS0 was found to be inactive, whereas TSR5 and TSP10 were able to degrade a significant amount of venlafaxine. Figure 9 displays the degradation curves of venlafaxine using these materials as photocatalysts.

Table 2. Average weight percentage and atomic abundance, estimated by EDX, of C, O, Si, and Ti in the reference, TSR5 and TSP10 materials.

Material	C		O		Si		Ti	
	Weight [%]	Atomic	Weight [%]	Atomic	Weight [%]	Atomic	Weight [%]	Atomic
TS0	7.86	12.15	54.41	63.23	35.77	23.77	0.94	0.36
TSM5	5.63	8.92	53.34	63.53	39.73	27.00	0.90	0.36
TSP5	4.96	7.86	55.14	65.59	37.98	25.74	1.36	0.54
TSP5h	9.59	14.61	54.57	62.37	34.51	22.47	0.88	0.34
TSP10	7.48	11.33	59.35	67.48	31.96	20.70	0.88	0.33

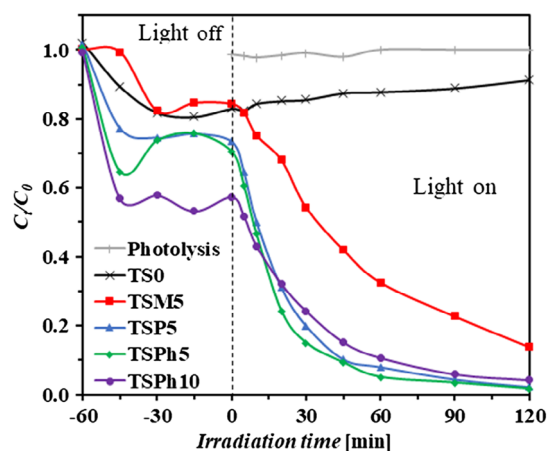


Figure 9. Photodegradation of venlafaxine under simulated solar irradiation with the reference, TSR5, and TSP10 materials. Experimental conditions: $[\text{Venlafaxine}]_0 = 5 \text{ mg L}^{-1}$, photocatalyst load = 1 g L^{-1} , and incident photon irradiance $I = 500 \text{ W m}^{-2}$.

The curves shown in Figure 9 show that the materials adsorbed part of the venlafaxine from the solution prior to the irradiation. After 1 h in the absence of light, TSM5 adsorbed a similar amount of venlafaxine than the reference (16% and 19%, respectively), while TSP5 and TSP5h adsorbed more (28% and 30%, respectively) and TSP10 the greatest amount (42%), expected as the volume of interparticle macropores is the highest for this material. Once the adsorption equilibrium was reached, the photocatalytic cycle was performed. Remarkably, the reference material was not photoactive, but all the selected new materials yielded quantitative photodegradation of venlafaxine in 2 h: TSM5 degraded 86%, while TSP5, TSP5h, and TSP10 degraded practically all the venlafaxine in solution (98%, 98%, and 96%, respectively). Besides the common products of the mineralization of organic pollutants by photocatalytic processes (CO₂ and H₂O), high-performance liquid chromatography (HPLC) analysis confirmed the presence of a small quantity of a degradation intermediate at a retention time of ≈ 1.6 min, which was identified as atenolol. As an example, Figure S8, Supporting Information, shows the HPLC chromatogram profile for the degradation of venlafaxine using TSP5h as the photocatalyst. Furthermore, low-molecular-weight molecules such as oxalic, maleic, and formic acids were also detected in very low concentrations.

Once the first photocatalytic cycle was performed to determine that the materials were photoactive, to study and properly compare the photoactivity efficiency of the titanium silicalites, another photocatalytic run was performed, considering the amount of adsorbed venlafaxine of each material prior to the photodegradation, to ensure that the initial concentration before photocatalysis was kept at $\approx 5 \text{ mg L}^{-1}$. Figure 10 exhibits the photodegradation curves of venlafaxine after adsorption equilibria (left) and the pseudo-first-order kinetic adjustment (right). The calculated kinetic parameters are displayed in Table 3.

Due to the higher initial concentration at the start of venlafaxine photodegradation compared to the first photocatalytic cycle (Figure 9), the degraded molar percentage was slightly lower:

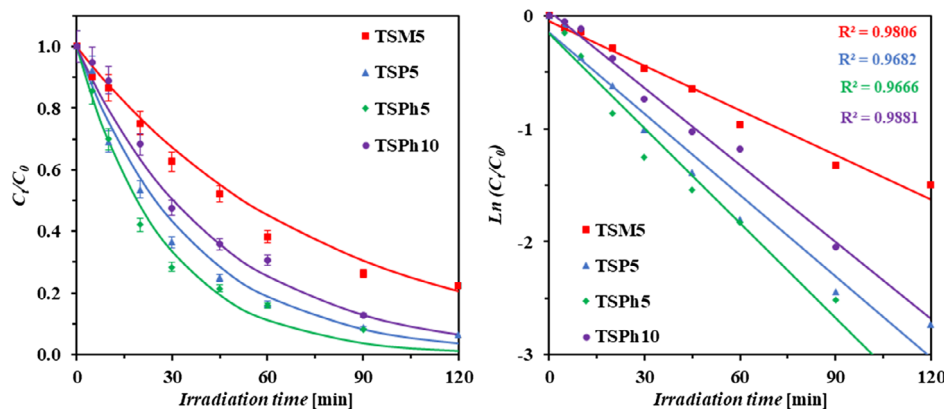


Figure 10. Photodegradation of venlafaxine after adsorption equilibria ($[\text{Venlafaxine}]_0 = 5 \text{ mg L}^{-1}$) and pseudo-first-order kinetic adjustment of the photodegradation process.

Table 3. Kinetic constants calculated from venlafaxine degradation curves.

Catalyst [l g L^{-1}]	k^a [min^{-1}]	$t_{1/2}^b$ [min]
TSM5	0.013	52.53
TSP5	0.028	24.87
TSPH5	0.036	19.09
TSPH10	0.023	30.44

^a) Degradation rate constant; ^b) Half-life time.

78%, 93%, 92%, and 87% for TSM5, TSP5, TSPH5, and TSPH10, respectively. TSM5 yielded a lower degradation rate among the tested materials, consistent with its similar UV–vis absorbance spectra and PL at $\lambda_{\text{ex}} = 370 \text{ nm}$ to those of the reference. Comparing TSPH5 and TSPH10 (materials prepared with the same organotriethoxysilane), the performance of the latter is poorer, probably due to a loss of crystallinity, a greater particle size, and lower mesopores and total pore volume. TSPH5 and TSP5 exhibit similar photocatalytic activity and are the best among the tested materials. However, from among the two samples, photocatalytic degradation of the pollutant was faster with the TSPH5, with a rate constant threefold higher than that of the TSM5 sample and with a half-life time reduced by almost three times. This could be related to the higher specific surface area and amount of TiO_6 observed in the UV–Raman spectra of TSPH5 compared to TSP5. Although in the literature tetra-coordinated TiO_4 species are said to be more active than octahedral TiO_6 species, in the case of the materials synthesized in this study, the latter is more superficial and therefore more accessible to the pollutant, which implies an improvement in the kinetics of degradation.

3. Conclusion

Three series of titanium silicalites (TSR%) prepared by a modified hydrothermal synthetic strategy have been obtained. The modification of the method consisted of the addition of an organotriethoxysilane, RTEOS (where R = methyl, propyl or phenyl),

at various molar percentages with respect to tetraethoxysilane (TEOS) in an attempt to direct the nanostructuring and to obtain modified titanium silicalites bearing a variety of morphologies and textural properties with the aim of improving their photocatalytic activity. XRD patterns and FTIR spectra confirmed that TSR5 and TSR10 exhibited a crystalline zeolite structure, whereas the addition of higher amounts of RTEOS resulted in amorphous or semicrystalline materials. Their XRD patterns together with their UV–vis spectra were consistent with the absence of anatase, the latter indicating also the presence of extraframework hexacoordinated titanium. It should be noted that a wider spectral range in UV–vis absorption closer to the visible spectral range was observed for these materials. Materials displaying a lower intensity emission in their PL spectra than the reference (TSP5, TSPH5, and TSPH10) were considered better photocatalysts due to a slower hole–electron recombination rate, which was later confirmed in the photodegradation of venlafaxine. These initial photocatalytic studies revealed that, in contrast to the reference, TSR5 and TSPH10 were photoactive under simulated solar irradiation. Surprisingly, the TSP5 and TSPH5 materials, which exhibit the smallest and most homogeneous pore diameter, as well as the smallest particle size, were the most photoactive of all the series, evidencing how the porous texture is a crucial parameter in their photocatalytic properties. Thus, after this in-depth textural, morphological, and chemical study, it can be stated that the proposed synthetic approach yields modified titanium silicalites with improved photocatalytic properties, which efficiently degrade venlafaxine, leading the way to further studies for their optimization.

4. Characterization Methods and Parameters of the Photocatalytic Tests

This section gathers a brief description of the methods and equipment employed for the characterization of the materials. For detailed measurements and calculation methods of textural parameters see Section S6, Supporting Information.

XRD patterns were acquired using a PANalytical Empyrean XRD instrument (Empyrean, Almelo, The Netherlands) with a

copper-rotating anode and a graphite monochromator. FTIR spectra were obtained using a Jasco spectrometer (mod. 4700, Japan). UV–vis DRS were recorded using a Jasco UV–vis spectrometer (mod V-560, Rev. 1.00) and BaSO₄ as reference material. PL spectra were acquired using a Jasco spectrofluorometer (mod FP-8300) equipped with a 150 W xenon lamp. UV–vis Raman spectra were obtained using a Raman Jasco spectrometer (mod NRS-5100). The skeletal density of TS materials was obtained using a helium pycnometer (AccuPyc 1330, Micromeritics, Norcross, GA, USA). N₂ (−196 °C) and CO₂ (0 °C) adsorption isotherms were obtained using a volumetric adsorption system (ASAP2020, Micromeritics, Norcross, GA, USA). PSD were calculated according to DFT using SAIEUS method and software.^[52] FESEM micrographs were obtained at 200 kV with a Carl Zeiss MERLIN field-emission scanning electron microscope (Carl Zeiss SMT, Oberkochen, Germany). The instrument was equipped with an energy-dispersive X-ray (EDX) detector (Oxford Inca Energy 350X-MAX 50, Oxford Instruments, Abingdon, UK).

All the photodegradation experiments of venlafaxine were performed in ultrapure water (18.2 MΩ.cm), with 50 mL of contaminant solution (5 mg L^{−1}), under magnetic stirring, continuously purged with airflow, a fixed photocatalyst dose of 1 g L^{−1}, and 2 h under simulated solar light using a Solarbox 1500e (CO.FO.ME.GRA) equipped with a 1500 W xenon lamp (500 W m^{−2}). During the experiments, aliquots of 0.5 mL were taken with a 5 mL syringe and a 0.45 μm filter and poured into an HPLC insert. The venlafaxine concentration of the aliquots was determined by ultrahigh-pressure liquid chromatography using a Shimadzu Nexera X2 LC-30AD apparatus with an SPD-M20A diode array detector, equipped with a Kinetex XB-C18 100 Å column (100 × 2.1 mm; 1.7 μm particle diameter). An isocratic method with a mobile phase of 25/75 %v Acetonitrile/Ultrapur water (with 1 %v of formic acid) at a flow rate of 0.25 mL min^{−1} at 35 °C was used. The excitation wavelength for venlafaxine was 275 nm. In addition, the identification of common organic carboxylic acids was also assessed by HPLC (Hitachi Elite LaChrom apparatus equipped with a diode array detector).

Supporting Information

Supporting Information is available from the Wiley Online Library or from the author.

Acknowledgements

The authors gratefully acknowledge financial support from Ministerio de Ciencia e Innovación, Government of Spain (PID2020-113558RB-C42), and from portuguese national funds through FCT/MCTES (PIDDAC): LSRE-LCM, UIDB/50020/2020 (DOI: 10.54499/UIDB/50020/2020) and UIDP/50020/2020 (DOI: 10.54499/UIDP/50020/2020); and ALICE, LA/P/0045/2020 (DOI: 10.54499/LA/P/0045/2020). G.C.-Q thanks Ministerio de Universidades, Government of Spain, for a predoctoral grant within the Formación de Profesorado Universitario (FPU) program (FPU18/03467) and the Government of Navarra, for a predoctoral international mobility grant (0011-3564-2022-000035). M.J.S. acknowledges FCT funding under the Scientific Employment Stimulus - Institutional Call (CEECINST/00010/2021). M.V.L.-R acknowledges financial support from Ministerio de Ciencia e Innovación, Government of Spain

(PID2022-142169OB-I00), and from FEDER 2014-2020 Operative Program and Junta de Andalucía, Spain (FEDER-UJA-1380629). M.E.-V. thanks UPNA for the project Jóvenes Investigadores UPNA 2022 (PJUPNA18-2022). The authors would also like to thank the technical and human resources from UCTAI (Unidad Científico Técnica de Apoyo a la Investigación) at UPNA and the use of the “Centro de Instrumentación Científico-Técnica” at the University of Jaén.

Conflict of Interest

The authors declare no conflict of interest.

Author Contributions

G.C.-Q. took care of investigation and writing the original draft. M.J.S took care of methodology, investigation, and writing the review and editing. M.V.L.-R. took care of writing the review and editing. M.E.-V. took care of methodology, resources, and writing the review and editing. J.J.G. took care of conceptualization, supervision, project administration, funding acquisition, and writing the review and editing. C.G.S. took care of conceptualization, supervision, and writing the review and editing. J.L.F. took care of resources, supervision, funding acquisition, and writing the review and editing. All authors have read and agreed to the published version of the manuscript.

Data Availability Statement

The data that support the findings of this study are available from the corresponding author upon reasonable request.

Keywords

antidepressant drug degradation, modified titanium silicalites, organotriethoxysilanes, photocatalysis under solar radiation

Received: July 31, 2023

Revised: November 1, 2023

Published online: December 27, 2023

- [1] A. Krishnan, M. Yoosuf, K. Archana, A. S. Arsha, A. Viswam, *J. Energy Chem.* **2023**, *80*, 562.
- [2] S. Feizpoor, S. R. Pouran, A. Habibi-Yangjeh, *Mater. Sci. Semicond. Process.* **2023**, *162*, 107444.
- [3] L.-J. Wang, P.-Y. Dong, G.-L. Zhang, F.-M. Zhang, *Energy Fuels* **2023**, *37*, 6323.
- [4] Z. H. Jabbar, B. H. Graimed, A. A. Okab, M. A. Issa, S. H. Ammar, H. J. Khadim, Y. A. Shafiq, *Environ. Nanotechnol., Monit. Manage.* **2023**, *19*, 100765.
- [5] J. Mathew, N. John, B. Mathew, *Environ. Sci. Pollut. Res.* **2023**, *30*, 16817.
- [6] N. Mumtaz, A. Javaid, M. Imran, S. Latif, N. Hussain, S. Nawaz, M. Bilal, *Environ. Pollut.* **2022**, *308*, 119690.
- [7] J. Musial, D. T. Mlynarczyk, B. J. Stanisz, *Sci. Total Environ.* **2023**, *856*, 159122.
- [8] M. Wang, Y. Cai, B. Zhou, R. Yuan, Z. Chen, H. Chen, *Sci. Total Environ.* **2022**, *836*, 155652.
- [9] Y. Yu, H. Huang, *Chem. Eng. J.* **2023**, *453*, 139755.
- [10] S. Guo, Y. Ji, Y. Li, H. Li, P. An, J. Zhang, J. Yan, S. Liu, T. Ma, *Appl. Catal., B.* **2023**, *330*, 122583.

- [11] J. El hamdaoui, K. Lakaal, D. Mazkad, M. Beraich, A. El Fatimy, M. Courel, L. M. Pérez, P. Díaz, D. Laroze, E. Feddi, *Mater. Res. Bull.* **2023**, *164*, 112235.
- [12] M. R. Islam, M. S. Islam, M. Y. Zamil, N. Ferdous, C. Stampfl, J. Park, M. K. Hossain, *J. Phys. Chem. Solids* **2023**, *176*, 111263.
- [13] Q. Sun, Z. Li, J. Li, N. Liu, M. Zhang, T. Le, *J. Alloys Compd.* **2023**, *955*, 170234.
- [14] C. Liane Ücker, F. San Martins Rodrigues, R. de Gouveia Cantoneiro, V. Goetzke, E. Ceretta Moreira, M. Meneghetti Ferrer, C. Wienke Raubach, S. Cava, *J. Photochem. Photobiol., A* **2023**, *441*, 114694.
- [15] K. Villa, J. R. Galán-Mascarós, N. López, E. Palomares, *Sustainable Energy Fuels* **2021**, *5*, 4560.
- [16] D. Spasiano, R. Marotta, S. Malato, P. Fernandez-Ibañez, I. Di Somma, *Appl. Catal., B* **2015**, *170–171*, 90.
- [17] M. Taramasso, G. Perego, B. Notari, (Snamprogetti S.p.A., Milan, Italy), *US-4410501-A*, **1983**.
- [18] W. Wu, D. T. Tran, S. Cheng, Y. Zhang, N. Li, H. Chen, Y. H. (Cathy) Chin, L. Yao, D. Liu, *Microporous Mesoporous Mater.* **2021**, *311*, 110710.
- [19] G. Xiong, Q. Jia, Y. Cao, L. Liu, Z. Guo, *RSC Adv.* **2017**, *7*, 24046.
- [20] S. Du, H. M. Chen, H. X. Shen, J. Chen, C. P. Li, M. Du, *ACS Appl. Nano Mater.* **2020**, *3*, 9393.
- [21] M. G. Clerici, in *Metal Oxide Catalysis*, Vol. 2 (Eds: S. D. Jackson, J. S. J. Hargreaves), Wiley-VCH, Weinheim, Germany **2009**, Ch.18, <https://doi.org/10.1002/9783527626113.ch18>.
- [22] H. Yin, F. Su, C. Luo, L. Zhu, W. Zhong, L. Mao, K. You, D. Yin, *Appl. Catal., B* **2022**, *302*, 120851.
- [23] M. Zhu, C. Zhu, D. Wu, X. Wang, H. Wang, J. Gao, H. Huang, C. Shi, Y. Liu, Z. Kang, *Nanoscale* **2019**, *11*, 15984.
- [24] Z. Zhao, D.-G. Cheng, F. Chen, X. Zhan, *Int. J. Hydrogen Energy* **2020**, *45*, 33532.
- [25] S. P. D. Ormond, M. Ratova, P. Kelly, M. Edge, B. Mihailova, L. Tosheva, *J. Porous Mater.* **2016**, *23*, 1421.
- [26] Q. Shang, W. Chi, P. Zhang, Y. Ling, X. Liu, G. Cui, W. Liu, X. Shi, B. Tang, *Process Saf. Environ. Prot.* **2022**, *157*, 297.
- [27] Q. Wu, H. Wang, C. Yi, *Optik* **2018**, *158*, 1460.
- [28] N. Li, B. Yang, M. Liu, Y. Chen, J. Zhou, *Chin. J. Catal.* **2017**, *38*, 831.
- [29] H. Yamashita, K. Mori, *Chem. Lett.* **2007**, *36*, 348.
- [30] H. Yamashita, K. Mori, Y. Kuwahara, T. Kamegawa, M. Wen, P. Verma, M. Che, *Chem. Soc. Rev.* **2018**, *47*, 8072.
- [31] W. O. Parker, R. Millini, *J. Am. Chem. Soc.* **2006**, *128*, 1450.
- [32] M. Signorile, L. Braglia, V. Crocellà, P. Torelli, E. Groppo, G. Ricchiardi, S. Bordiga, F. Bonino, *Angew. Chem., Int. Ed.* **2020**, *59*, 18145.
- [33] Q. Guo, K. Sun, Z. Feng, G. Li, M. Guo, F. Fan, C. Li, *Chem. Eur. J.* **2012**, *18*, 13854.
- [34] Y. Wang, H. Yang, Y. Zuo, D. Tian, G. Hou, Y. Su, Z. Feng, X. Guo, C. Li, *Appl. Catal., B* **2023**, *325*, 122396.
- [35] A. Thangaraj, M. J. Eapen, S. Sivasanker, P. Ratnasamy, *Zeolites* **1992**, *12*, 943.
- [36] G. Li, N. M. Dimitrijevic, L. Chen, J. M. Nichols, T. Rajh, K. A. Gray, *J. Am. Chem. Soc.* **2008**, *130*, 5402.
- [37] B. Wang, Y. Guo, J. Zhu, J. Ma, Q. Qin, *Coord. Chem. Rev.* **2023**, *476*, 214931.
- [38] J. Gao, L. Gao, B. Zhang, H. Wang, W. Ma, *Can. J. Chem. Eng.* **2021**, *99*, S596.
- [39] P. Moriones, G. Arzamendi, A. Cornejo, J. J. Garrido, J. C. Echeverria, *J. Phys. Chem. A* **2019**, *123*, 10364.
- [40] Establishing a Watch List of Substances for Union-wide Monitoring in the Field of Water Policy Pursuant to Directive 2008/105/EC of the European Parliament and of the Council, COM (2022) 5098, Final, <https://eur-lex.europa.eu/legal-content/EN/TXT/?uri=CELEX%3A32022D1307> (accessed: April 2022).
- [41] Y. Shi, L. Chen, J. Li, Q. Hu, G. Ji, Y. Lu, X. Hu, B. Zhu, W. Huang, *Chem. Phys. Lett.* **2021**, *762*, 138116.
- [42] T. Armaroli, F. Milella, B. Notari, R. J. Willey, G. Busca, *Top. Catal.* **2001**, *15*, 63.
- [43] P. J. Launer, B. Arkles, in *Silicon Compounds: Silanes and Silicones*, 3rd ed. (Ed: G. L. Larson), Gelest, INC, Morrisville, PA **2013**, pp. 175–178, ISBN: 978-0-578-12235-9.
- [44] J. Tauc, *Mat. Res. Bull.* **1968**, *3*, 37.
- [45] C. Lamberti, S. Bordiga, D. Arduino, A. Zecchina, F. Geobaldo, G. Spanó, F. Genoni, G. Petrini, A. Carati, F. Villain, G. Vlaic, *J. Phys. Chem. B* **1998**, *102*, 6382.
- [46] M. Pera-Titus, J. Llorens, *Appl. Surf. Sci.* **2010**, *256*, 5305.
- [47] M. Thommes, K. Kaneko, A. V. Neimark, J. P. Olivier, F. Rodriguez-Reinoso, J. Rouquerol, K. S. W. Sing, *Pure Appl. Chem.* **2015**, *87*, 1051.
- [48] Ch. Baerlocher, L. B. McCusker, <https://asia.iza-structure.org/IZA-SC/framework.php?STC=MFI> (accessed: August 2022).
- [49] I. Díaz, E. Kokkoli, O. Terasaki, M. Tsapatsis, *Chem. Mater.* **2004**, *16*, 5226.
- [50] Y. Zuo, Y. Chen, T. Li, J. Yu, H. Yang, M. Liu, X. Guo, *Microporous Mesoporous Mater.* **2022**, *336*, 111884.
- [51] J. Li, F. Zhang, L. Zong, X. Wang, H. Wei, *Catalysts* **2021**, *11*, 113.
- [52] J. Jagiellot, *Langmuir* **1994**, *10*, 2778.